Human Endothelial Cells Internalize *Candida parapsilosis* via N-WASP-Mediated Endocytosis

Tatsushi Shintaku,[a]* Kyle A. Glass,[a] Matthew P. Hirakawa,[b] Sarah J. Longley,[a] Richard J. Bennett,[b] Joseph M. Bliss,[a,b,c] Sunil K. Shaw[a,c]

Department of Pediatrics, Women & Infants Hospital of Rhode Island, Providence, Rhode Island[a]; Graduate Program in Pathobiology, Brown University, Providence, Rhode Island[b]; Warren Alpert Medical School of Brown University, Providence, Rhode Island[c]

Candida parapsilosis is a frequent cause of disseminated candidiasis and is associated with significant morbidity and mortality. Although important in pathogenesis, interactions of this organism with endothelial cells have received less attention than those of *Candida albicans*. Internalization of *C. parapsilosis* by monolayers of human endothelial cells was examined in an *in vitro* assay and compared to that of *C. albicans*. Both live and heat-killed yeast were efficiently internalized, with heat-killed yeast subsequently being detected in an acidic subcompartment. Internalization was marked by a process of engulfment by thin membrane extensions from the endothelium. Efficiency of internalization differed among different clinical isolates and species of yeast. Opsonization of *C. parapsilosis* by serum factors was not sufficient to cause endocytosis; instead, serum appeared to directly stimulate endothelial uptake. Colocalization of endothelial actin and N-WASP at sites of *C. parapsilosis* internalization was observed. A Förster-resonance energy transfer (FRET) probe for N-WASP activity showed active N-WASP at sites of internalization for both live and heat-killed *C. parapsilosis* and *C. albicans*. An actin nucleation inhibitor (cytochalasin D) and an N-WASP inhibitor (wiskostatin) both inhibited uptake of heat-killed *C. parapsilosis*, as did short interfering RNA-mediated ablation of N-WASP. Thus, endocytosis by endothelial cells may represent a means of traversal of the blood vessel wall by yeast during disseminated candidiasis, and N-WASP may play a key role in the process.

*C*andida species are the most common organisms recovered from fungal infections in humans. Disseminated candidiasis is a frequent and serious complication among the immunocompromised, acutely ill patients, and premature neonates (1, 2). The mortality, morbidity, and increased hospital stays attributable to these infections provide a substantial financial and public health impact (3, 4). Historically, *Candida albicans* was the most frequent cause of these infections, accounting for 70 to 80% of isolates from infected patients (5). However, infections caused by non-*albicans Candida* species, including *C. glabrata* and *C. parapsilosis*, are increasing in frequency worldwide (6–8). In some centers, *C. parapsilosis* has emerged as the leading cause of invasive candidiasis, particularly in newborns (9, 10). The majority of studies related to pathogenesis of candidiasis have focused on *C. albicans* and, to a lesser extent, *C. glabrata*. Despite increasing recognition of *C. parapsilosis* as an important pathogen, its pathogenesis remains relatively underexplored.

For *Candida* to cause disseminated infection, it must adhere to and cross the blood vessel wall. However, the endothelium provides a nonadherent and nonthrombogenic surface to the circulation. Hematogenous pathogens must somehow be able to negotiate this obstacle. For *C. albicans*, some of the molecular pathways used to adhere to endothelium have been identified. *C. albicans* switches between a yeast and hyphal form, and both are required for virulence (11). *C. albicans* hyphae bind to endothelium much more efficiently than do yeast forms (12) in static adhesion assays. However, under conditions of fluid flow, which may be more appropriate to simulate actual adhesion in the bloodstream, *C. albicans* yeast forms bound more efficiently to endothelium (13). Several *C. albicans* adhesins have been identified, including the Als (agglutinin-like sequence) family (14–16). Als3p binds to N-cadherin, E-cadherin, gp96 heat shock protein, EGFR, and HER2 (17–19). In contrast to *C. albicans*, *C. glabrata* does not form true hyphae; instead, it forms elongated pseudohyphal structures. Ad-

hesion of *C. glabrata* occurs via Epa (epithelial adhesin) proteins, which bind to glycosyl ligands on epithelial and endothelial cells (20). *C. parapsilosis* is more closely related to *C. albicans* than to *C. glabrata*. Adhesion properties of *C. parapsilosis* have been less well studied than those of *C. albicans* and *C. glabrata*, but Als orthologs have been identified (21) which might play a similar role in adhesion.

Following adhesion, *C. albicans* uses endocytosis as an entry mechanism to invade epithelial and endothelial cells. Adhesion of Als3p to host cell surface receptors leads to internalization of hyphae. This process recruits host cell actin to hyphae and is blocked by cytochalasin D, an inhibitor of actin polymerization (22). Active penetration by hyphae of *C. albicans* has also been described, whereby growing hyphae damage the monolayer of cells and gain entry into deeper tissues (23).

In addition to hyphal internalization via Als3p, other internalization mechanisms have also been described. Multiple groups have demonstrated internalization of yeast forms (24–27) by epithelial or endothelial cells *in vitro*. Furthermore, *C. albicans* isolates that have been trapped in the yeast form using genetic ma-

nipulations are also capable of disseminating to and colonizing organs in animal models, indicating that yeast forms can be invasive *in vivo* (11). Interestingly, in some reports, there is evidence for host cell projections (pseudopods or lamellipodia) that extend from the cell to envelop yeast (25, 27). Recently, endocytosis of *C. albicans* hyphae has been reported to be dependent on cortactin, an actin nucleation promotion factor, as well as clathrin and dynamin, parts of the endocytic machinery (28). In this study, we examined internalization of *C. parapsilosis* yeast by endothelial cells *in vitro* and compared and contrasted it to that of *C. albicans*.

MATERIALS AND METHODS

Endothelial cells. Primary human umbilical vein endothelial cells (HUVEC) were obtained from Lonza (Hopkinton, MA) and grown according to the manufacturer's instructions in EGM-2 medium at 37°C and 5% CO_2. Cells were used between passages 3 and 5. For imaging studies, HUVEC were grown in 8-well chambered coverglass slides (Nunc Labtek II) or coverglass-bottomed dishes (MatTek Corp., Ashland, MA) coated with fibronectin.

Adenoviruses. cDNAs encoding green fluorescent protein (GFP)-actin (29), GFP-N-WASP (30), and N-WASP biosensor (31) were cloned into an adenovirus (AdV) type 2 expression vector (32) and used to infect HUVEC as previously described (33). Experiments were done under the oversight of an institutional recombinant DNA committee and in compliance with NIH guidelines.

Yeast strains and media. *C. parapsilosis* strains used in this study include the clinical commensal isolate Ro75-R1 (34) and four clinically invasive isolates, WIH03, 14-72931-101 (referred to here as JMB81), 14-72101-101 (JMB72), and 13-70091-101 (JMB77) (35). Additional strains included *C. albicans* SC5314 and *S. cerevisiae* W303. Strains were maintained on YPD agar (1% yeast extract, 2% peptone, 2% dextrose, 2% agar). Overnight cultures were grown in YPD broth for 16 h with vigorous agitation at 37°C (or 30°C for *S. cerevisiae*). Induction of *C. parapsilosis* was achieved by resuspending washed yeast after overnight culture in Medium 199 (Lonza) at 3×10^6 yeast/ml and incubating for an additional 3 h at 37°C. Induction of *C. albicans* hyphae was similar, but for only ~90 min, and aliquots were sampled every 10 min for germ tube formation by bright-field microscopy. For heat killing, yeast were incubated at 65°C for 30 min with occasional mixing to reduce clumping. Heat-killed yeast were routinely cultured on YPD agar and incubated at 37°C overnight to confirm killing.

pHrodo labeling. Heat-killed yeast were suspended in Hanks balanced salt solution plus Ca and Mg (HBSS+/+) and adjusted to 3×10^7 yeast/ml. The biosensor pHrodo-succinimidyl ester (Invitrogen, Grand Island, NY) was added at 0.05 mM for 45 min. After staining, pHrodo-labeled yeast were centrifuged at 2,100 relative centrifugal force (RCF), washed once with 3% bovine serum albumin (BSA), and washed three times with HBSS. Labeled yeast were stored in HBSS at −80°C, and a fresh aliquot was thawed for each experiment. To test for pH sensitivity, pHrodo-stained yeast were incubated in HBSS or in 100 mM sodium acetate, pH 5, and loaded onto coverglass slides for imaging. Exactly 50 yeast cells were selected from each condition, and their mean fluorescence intensities were quantified. The median intensity for each condition was calculated (see Fig. 1c).

Internalization assays. pHrodo-labeled yeast were diluted into EGM-2 medium (containing 2% serum), added to confluent monolayers of HUVEC in 8-well chambered cover slides, and incubated at 37°C, 5% CO_2 for the indicated time. A yeast/HUVEC ratio of 50:1 was used to ensure that an excess of yeast was available. For serum starvation experiments, monolayers were grown to confluence in EGM-2, the medium was replaced with EBM-2 (base medium, containing no serum), and pHrodo-stained yeast were added. Endothelial monolayers remained relatively intact by bright-field microscopy for up to 24 h under serum starvation but started to show cell loss beyond this time period. For imaging of internalization, monolayers were scanned under bright-field conditions to ensure

that only confluent areas were imaged. After image acquisition, red channel images were digitally thresholded to select for pHrodo-positive yeast, and the same threshold value was applied across the entire image stack. For quantification of internalization, 8 randomly selected fields of view were imaged, the thresholded area of internalized yeast was calculated, and data were exported from MetaVue to Excel. Results shown in Fig. 3a to d are expressed as an internalization index, where 100 represents the theoretical ideal of the 20× field of view entirely filled with pHrodo-bright yeast. Wiskostatin (EMD Biosciences) was used at a final concentration of 2.5 μM. Cytochalasin D (Sigma) was used at a final concentration of 0.5 μM. Drugs were added at the same time as pHrodo-stained yeast and were present throughout the assay. Monolayers were evaluated by phase-contrast or differential contrast (DIC) imaging and confirmed to be intact prior to imaging. For these experiments and for short interfering RNA (siRNA) results, internalization was normalized to the control to permit pooling of results from multiple independent experiments.

Statistical analysis. Nonparametric data generated from pHrodo fluorescence and internalization assays were analyzed using Mann-Whitney rank-sum tests or Kruskal-Wallis analysis of variance on ranks for 2-group or multiple-group comparisons, respectively. In each reported Kruskal-Wallis analysis, the overall P value was <0.001 in all cases. Between-group comparisons were made by the Dunn's method, with P values of <0.05 considered significant (SigmaPlot version 11.0 statistical software).

Calcofluor white staining of yeast. Calcofluor white (Sigma) stock was made in water at 5 mM. Yeast were labeled at 5 μM at room temperature for 10 min and then washed three times with HBSS+/+ to remove excess stain.

Microscopy and imaging. Images were obtained with a Nikon inverted microscope (TE2000E) equipped with a charge-coupled-device (CCD) camera (Roper Coolsnap HQ) and excitation and emission filter wheels (Prior Proscan II). A stage incubator (20-20 Technologies Inc., Wilmington, NC) at 37°C and 5% CO_2 was used for live cell imaging. Microscope control and image acquisition was via MetaVue 6.42r6 software (Molecular Devices, Sunnyvale, CA). Images were overlaid and further analyzed in ImageJ 1.45s (National Institutes of Health). Figures were created and edited in Photoshop Elements 6.0 (Adobe Systems Inc.). All changes made to contrast were linear.

z-series image acquisition. HUVEC were cultured in an 8-well glass-bottom chamber slide (Lab-Tek II chambered coverglass), infected with an adenovirus expressing GFP prior to addition of pHrodo-labeled yeast, and cultured overnight at 37°C and 5% CO_2. Postincubation, cells were imaged with a 60× Plan Apo oil immersion objective lens, and z-series images were collected at 0.5-μm intervals. Images were deconvolved using AutoQuant 9.3.

FRET. HUVEC were infected with N-WASP biosensor AdV and imaged 3 days postinfection. Live, induced yeast or pHrodo-labeled, heat-killed yeast were washed twice in HBSS+/+, resuspended in EGM-2, and added to separate dishes at 3×10^6 yeast/dish. For imaging of endothelial cell uptake of yeast and N-WASP activity, live time-lapse imaging was employed and sequential images were collected with a 20× Plan Apo objective lens in cyan fluorescent protein (CFP) (donor image), CFP-yellow fluorescent protein (YFP) (Förster-resonance energy transfer [FRET] image), and DsRed (pHrodo) channels with a Chroma 86006 CFP/YFP/DsRed filter set (Chroma Technology Corp., VT). CFP was excited using a 436/10 filter, and the fluorescence was detected with a 492/18 (donor image) or 580/20 (FRET image) emission filter. For pHrodo, excitation S465/30 and emission 630/60 filters were used. For FRET imaging, exposure times were adjusted depending on the expression level of N-WASP biosensor and were between 100 and 500 ms. The exposure time used for pHrodo was 5 ms. Bleedthrough of pHrodo to all other channels was measured and found to be minimal. After time-lapse imaging was complete, the background was subtracted from each image and an N-WASP activation profile was generated in ImageJ by digitally dividing the individual pixel intensities of the donor image by the FRET image (inverse
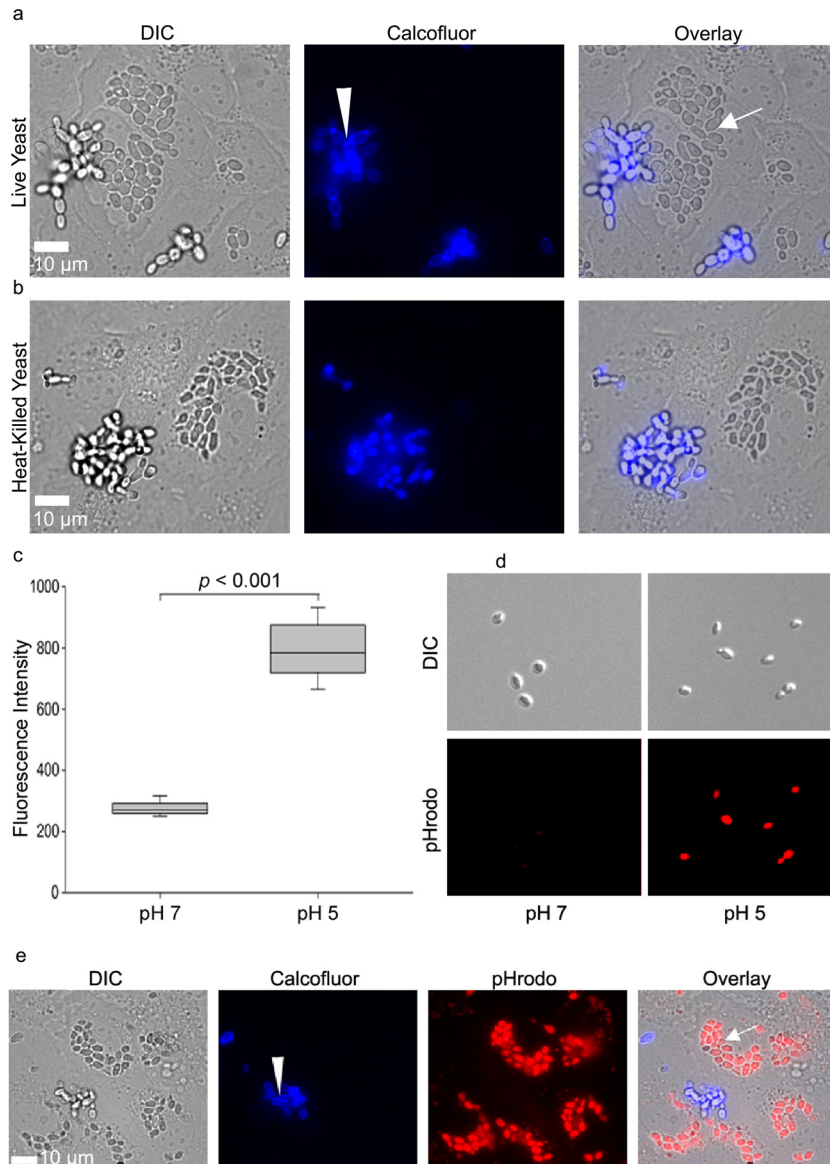
FIG 1 (a) Live *C. parapsilosis* JMB81 cells were internalized by endothelial cells. Panels on the left show differential interference contrast (DIC) images, with extracellular yeast visible as bright grape-like clusters. Intracellular yeast are visible as darker oval clusters. Middle panels show calcofluor staining of extracellular yeast in blue (arrowhead). Panels on the right show the overlay, where intracellular yeast remained unstained by calcofluor (arrow). (b) Heat-killed *C. parapsilosis* JMB81 cells were internalized by HUVEC. (c) pHrodo-labeled *C. parapsilosis* JMB81 was a sensitive bioindicator for pH. The mean fluorescence intensities of 50 pHrodo-labeled yeast cells were measured for each condition. The graph represents the medians, 25th and 75th percentiles (boxes), and 10th and 90th percentiles (whiskers). (d) Representative images showing the increase in pHrodo fluorescence observed at pH 5. (e) pHrodo-labeled heat-killed *C. parapsilosis* (JMB81) cells were internalized by HUVEC into an acidic subcompartment. The left panel shows a DIC image, with extracellular yeast visible as bright grape-like clusters and intracellular yeast visible as darker ovals. The second panel shows blue calcofluor staining of extracellular yeast (arrowhead). The third panel shows bright red pHrodo staining of intracellular yeast. For clarity, contrast has been adjusted to effectively threshold out pHrodo-dim extracellular yeast. The right panel shows the overlay, with intracellular yeast visible as pHrodo positive and calcofluor negative. Extracellular yeast remained calcofluor positive and pHrodo dim.

dynamic FRET). Results shown in Fig. 7 and 8 depict panels of representative slices from each movie. FRET calibration bars were generated with the LUT editor plugin for ImageJ.

siRNA transfection and Western blotting. N-WASP oligonucleotides (predesigned Silencer select siRNA) were purchased from Invitrogen and used as an equimolar pool of all three oligonucleotides. HUVEC were plated in 8-well chambers in EGM-2 without antibiotics. The next day, 30 pmol of siRNA and 0.3 μl of lipid-based transfection reagent (Dharmafect 4; Thermo Fisher Scientific) were added according to the manufacturer's protocol. The transfection mixture was removed after 24 h, and the cells

were further cultured until use in pHrodo internalization assays or Western blotting. For Western blotting, cells were lysed in 50 μl of hot (95°C) Laemmli buffer and resolved by SDS-PAGE (Nupage Novex 4 to 12% BisTris; Invitrogen). After transfer to nitrocellulose, membranes were probed with antibodies against N-WASP (Cell Signaling Technology, Beverly, MA) and imaged by chemiluminescence (Pierce PicoWest; Thermo Fisher Scientific). Membranes were subsequently reprobed with anti-actin antibody (Millipore, Billerica, MA).

SEM. HUVEC were grown to confluence on fibronectin-coated 12-mm glass coverslips. Live induced *C. parapsilosis* cells were added in
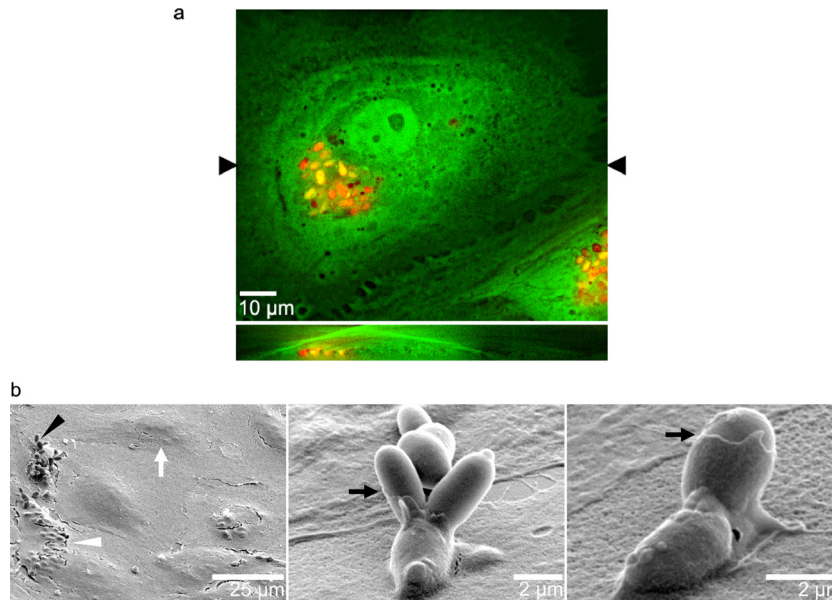
FIG 2 (a) pHrodo-bright *C. parapsilosis* cells were located within the endothelial cytoplasm, under the apical membrane. Endothelial cells expressing GFP in their cytoplasm were incubated overnight with heat-killed, pHrodo-labeled yeast (JMB81). (Top) Collapsed z-stack (*x-y*) showing pHrodo yeast as clusters of red and orange ovals, depending on the amount of cytoplasmic GFP. (Bottom) Orthogonal slice (*x-z*) at the level of the black arrowheads in the *x-y* view shown above, showing red and orange yeast present within the green endothelial cytoplasmic GFP. The image is representative of 5 independent experiments. (b) Scanning EM showed that *C. parapsilosis* (JMB81) was enveloped by thin cytoplasmic extensions from endothelial cells. In the left panel, a low-power view shows endothelial cells as larger mound-like shapes (white arrow). Intracellular yeast are visible as smaller mounds (white arrowhead). Extracellular adherent yeast are branching clusters (black arrowhead). Middle and right panels show higher magnifications of yeast adhering to the endothelial surface, with thin membranes covering their lower aspects (black arrows).

EGM-2 and incubated at 37°C for 2 h. Medium was then removed, and monolayers were rinsed in HBSS, fixed with 2.5% (wt/vol) glutaraldehyde in 0.1 M Na-cacodylate buffer, pH 7.4, at 4°C, and washed with 0.1 M Na-cacodylate buffer, pH 7.4. The cells were postfixed with 1% aqueous osmium tetroxide in 0.1 M Na-cacodylate buffer, pH 7.4, at 25°C for 90 min and washed with 0.1 M Na-cacodylate buffer, pH 7.4. Following fixation, cells were dehydrated with a 15% graded ethanol series and subsequently dried in a critical point dryer. The samples were then coated with 20 nm of gold/palladium (60:40) in an Emitech K550 sputter coater. Cells were imaged with a Hitachi S-2700 scanning electronic microscope (SEM) and collected with Quartz PCI software.

RESULTS

Endothelial cells internalize live and dead yeast. Primary human umbilical vein endothelial cells (HUVEC) grown to confluent monolayers are a widely used model of vascular endothelium. These monolayers form a semipermeable barrier to fluid and macromolecules and facilitate leukocyte diapedesis under inflammatory conditions. To determine whether endothelial cells internalize *C. parapsilosis*, HUVEC monolayers were coincubated overnight with live yeast (JMB81). Calcofluor is a cellulose- and chitin-specific fluorescent dye that binds to yeast cell walls but is excluded from endothelial cells. Following incubation, calcofluor was added to identify extracellular yeast (Fig. 1a, arrowhead). Intracellular yeast did not contact the dye and remained unstained (arrow). Clusters of unstained yeast were observed; apparently, they were within the endothelial cytoplasm. In a parallel experiment, heat-killed *C. parapsilosis* was also taken up by endothelial cells, indicating that uptake is not dependent on active penetration by the yeast (Fig. 1b).

Heat-killed yeast are endocytosed into an acidic compartment. To further investigate the properties of endothelial endocytosis, the pH-sensitive dye pHrodo was used to label heat-killed *C. parapsilosis* yeast (JMB81). As expected, pHrodo-labeled yeast showed a 2.5-fold increase in fluorescence intensity at pH 5 compared to that at pH 7, confirming their pH sensitivity (Fig. 1c and d). In the current study, pHrodo labeling was only applied to heat-killed yeast. When pHrodo-labeled yeast were incubated with endothelial cells and calcofluor was added after incubation, distinct nonoverlapping populations of pHrodo-positive (Fig. 1e, overlay, arrow) or calcofluor-positive (Fig. 1e, arrowhead, blue channel) yeast were observed, suggesting that internalized yeast were in an acidic intracellular compartment (termed pHrodo bright). When GFP-expressing HUVEC were incubated with heat-killed, pHrodo-labeled yeast, z-stack imaging confirmed that pHrodo-bright yeast were located under the endothelial cell apical surface and within its cytoplasm (Fig. 2a).

Intact monolayers of endothelial cells following incubation with live *C. parapsilosis* yeast were observed with scanning electron microscopy, and they were visible as rounded mounds 25 to 50 μm in size (Fig. 2b, left, white arrow). Occasional clusters of internalized yeast appeared as clusters of smaller (2 to 4 μm) mounds (Fig. 2b, left, white arrowhead). These probably correspond to the clusters of internalized yeast observed in fluorescence imaging (Fig. 1a, b, and e). Adherent yeast that were not yet internalized were scattered over the monolayer (Fig. 2b, black arrowhead). Closer examination of these adherent yeast frequently showed a thin membrane partly covering the lower yeast cell bodies, representing the endothelial cell membrane with a sheet-like or lamellipodial structure (black arrows, middle and right).

To quantify internalization of yeast, pHrodo staining of heat-
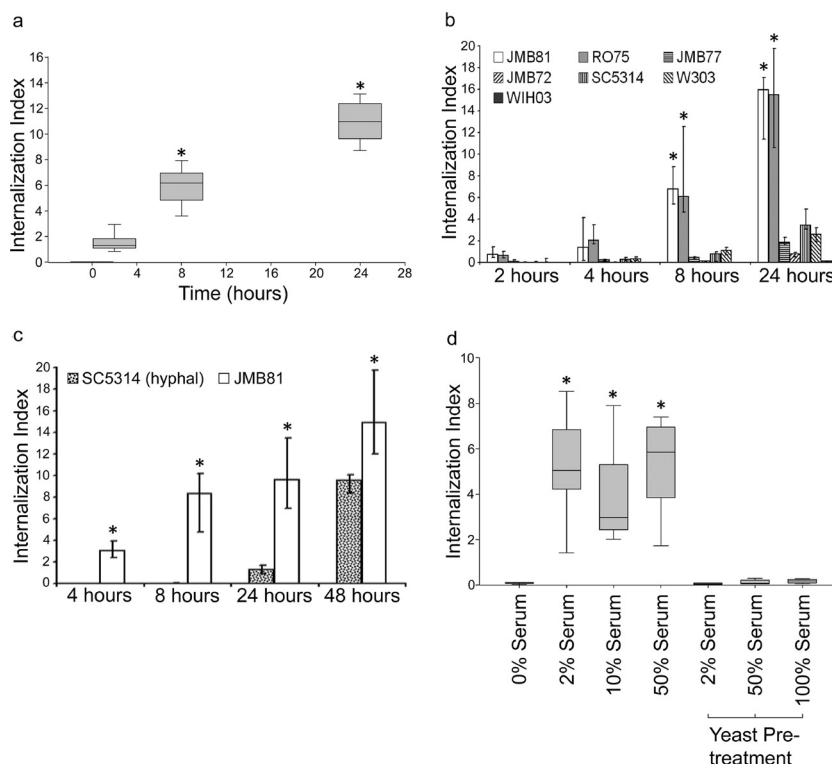
FIG 3 (a) Yeast (*C. parapsilosis* JMB81, heat killed and pHrodo labeled) were internalized over a 24-h period. An internalization index of 100 corresponds to a theoretical ideal of the field of view being completely filled with internalized yeast. The graph represents the medians, 25th and 75th percentiles (boxes), and 10th and 90th percentiles (whiskers). Data are from 5 independent experiments. *, $P < 0.05$ versus data at 0 h. (b) Different isolates of heat-killed and pHrodo-labeled yeast were taken up with differing efficiency. The graph represents the medians (bar) with 25th and 75th percentiles (error bars). Data are from 4 independent experiments. *, $P < 0.05$ versus JMB72, JMB77, and WIH03. (c) pHrodo-labeled, heat-killed *C. albicans* SC5314 hyphae were taken up with lower efficiency than was *C. parapsilosis* JMB81. The graph represents the medians (bar) with 25th and 75th percentiles (error bars). Data are from 3 independent experiments. *, $P < 0.05$ for SC5314 versus JMB81 at all time points. (d) Endothelial cells required serum for efficient uptake of heat-killed, pHrodo-labeled *C. parapsilosis*. However, pretreatment of yeast followed by washing away of serum did not result in appreciable internalization. The graph represents the medians, 25th and 75th percentiles (boxes), and 10th and 90th percentiles (whiskers). Data are from 4 independent experiments. *, $P < 0.05$ versus 0% serum.

killed *C. parapsilosis* was used to positively identify yeast that had been trafficked to an acidic compartment. In a time course experiment, internalized yeast were detectable 2 h after coincubation, rising in numbers for up to 24 h (Fig. 3a). Because the yeast were heat killed prior to pHrodo labeling, this increase represents ongoing endocytosis rather than proliferation of intracellular yeast. After 24 h, the number of internalized yeast fluctuated irregularly, possibly due to shedding of endothelial cells from the monolayer. If these endothelial cells contained internalized yeast, they would no longer be in the focal plane or field of view after shedding; thus, they would be omitted from the measurement. Although similar experiments were performed with live *C. parapsilosis*, active reproduction within endothelial cells was not observed; however, huge proliferation occurred with extracellular yeast (Fig. 4 shows an example; also see Movie S1 in the supplemental material).

When different heat-killed clinical isolates of yeast were compared, two isolates of *C. parapsilosis* showed the greatest internalization (Ro75 and JMB81) (Fig. 3b). Other isolates of *C. parapsilosis*, and the laboratory strains *C. albicans* SC5314 (yeast form) and *Saccharomyces cerevisiae* W303, showed a much smaller degree of uptake in this assay. Because *C. albicans* hyphae adhere more efficiently to endothelium under static conditions than the yeast form (12), we also compared internalization of heat-killed, pHrodo-labeled SC5314 hyphae to that of induced JMB81

(Fig. 3c). In this assay, SC5314 was internalized at a lower rate, particularly in the first 24 h of coincubation. Between 24 and 48 h, greater internalization occurred but still did not achieve the same level of internalization as JMB81. The presence of bovine serum was necessary for endocytosis of heat-killed *C. parapsilosis*, but endocytosis rates were similar over a range of 2 to 50% serum. Surprisingly, if the yeast were pretreated with serum for 1 h and excess serum was removed by washing, no uptake was observed, implying that opsonization of JMB81 by serum factors was not sufficient for endocytosis (Fig. 3d).

The actin cytoskeleton plays a role in yeast endocytosis. To identify the cytoskeletal mechanisms responsible for *C. parapsilosis* endocytosis, endothelial cells were labeled with GFP-actin, and live-cell imaging was used to monitor the process of internalization. Clusters of GFP-actin were observed in adherent and internalizing JMB81 yeast, suggesting a role for actin microfilaments in this process (Fig. 4, white arrows; also see Movie S1 in the supplemental material). Treatment with low doses of cytochalasin D, a potent cell-permeable inhibitor of actin polymerization, strongly decreased internalization of heat-killed, pHrodo-labeled yeast (Fig. 5a), further indicating that actin polymerization was important in the process.

N-WASP plays a role in yeast endocytosis. GFP-labeled N-WASP was used to determine if this actin nucleation promotion
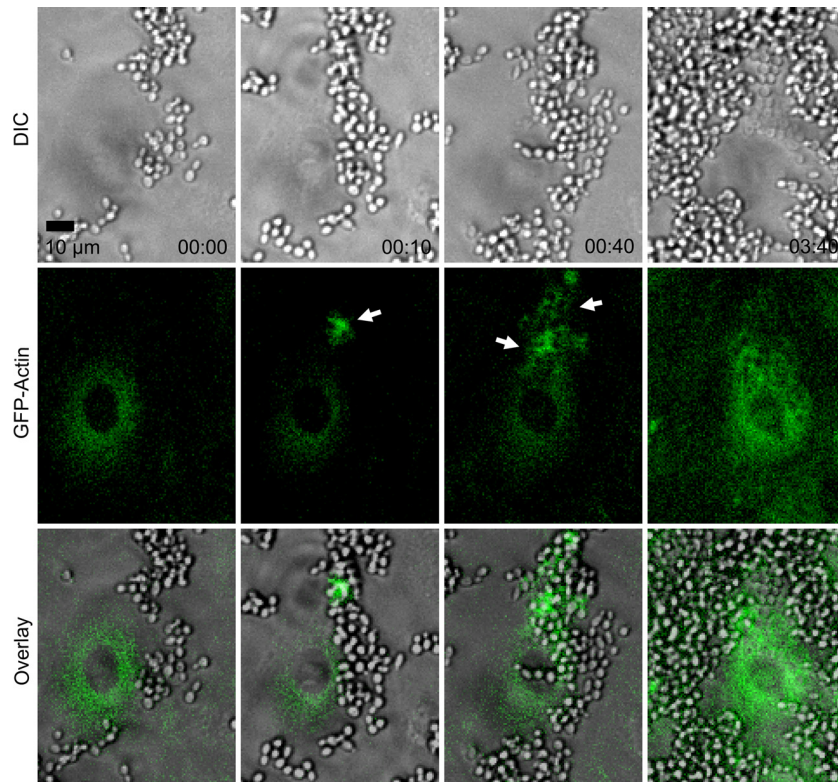
FIG 4 GFP-actin clustered around internalizing live *C. parapsilosis* (JMB81). The top row shows DIC images, the middle row shows GFP-actin, and the bottom row shows overlays. Actin clusters are shown by white arrows. Time is shown in hours and minutes. Movie S1 in the supplemental material shows the same sequence. Note the extensive proliferation observed with external yeast over the time course. Image sequences are representative of 5 independent experiments.

factor played a role in endocytosis. Live cell imaging showed endothelial cells with clusters of GFP-N-WASP at sites of *C. parapsilosis* internalization (Fig. 6, white arrows; also see Movie S2 in the supplemental material). Inhibition of N-WASP with wiskostatin, a cell-permeable N-WASP inhibitor (36), caused a significant decrease in heat-killed, pHrodo-labeled *C. parapsilosis* internalization (Fig. 5b). However, wiskostatin may have cellular targets other than N-WASP. A role for N-WASP in endocytosis was further interrogated using an N-WASP FRET biosensor. Live cell dynamic FRET imaging showed strong endothelial N-WASP activity around adherent and internalizing live *C. parapsilosis* JMB81 (Fig. 7a, white arrows; also see Movie S3 in the supplemental material). Using heat-killed, pHrodo-labeled *C. parapsilosis*, N-WASP activity was observed both prior to and after yeast internalization into the acidic compartment (Fig. 7b, white arrows; also see Movie S4 in the supplemental material). Broadly similar results were observed with *C. albicans* hyphae. Live SC5314 showed efficient adhesion to endothelium shortly after hyphal germination, and adhesion sites were marked by N-WASP activity, which persisted through the process of internalization and beyond (Fig. 8a, white arrows). Initially, adhesion to endothelium was via the growing germ tube, and FRET was observed at the attachment site but not at the unattached mother yeast (Fig. 8a, inset 1). Later, as the yeast was engulfed, FRET extended around both germ tubes and mother cells (Fig. 8a, inset 2). Heat-killed, pHrodo-labeled SC5314 hyphae were internalized much less efficiently and also more slowly (Fig. 3c). Nevertheless, N-WASP activity was also associated with those hyphae that did show internalization, and it

persisted until the hyphae became pHrodo bright (Fig. 8b). This result indicates that persistent N-WASP activity is associated with internalization for *C. parapsilosis* and *C. albicans*. To confirm the role for N-WASP in internalization, siRNA transfection was used to transiently knock down protein expression (Fig. 5d). Silencing of N-WASP expression also caused a significant decrease in heat-killed, pHrodo-labeled *C. parapsilosis* internalization compared to that of cells transfected with a control siRNA (Fig. 5c).

DISCUSSION

During hematogenous dissemination of pathogenic *Candida*, yeast travel through the bloodstream and invade tissues at sites that are anatomically distant from the original infection. To do this, they must adhere to and cross vessel walls. We show here that specific isolates of *C. parapsilosis* yeast forms are rapidly and efficiently taken up by monolayers of tightly packed endothelial cells. Uptake did not require activity on the part of the yeast; instead, heat-killed yeast were rapidly internalized, indicating active endocytosis or phagocytosis by endothelial cells.

Not all isolates of *C. parapsilosis* showed equal uptake by endothelial cells. It is possible that this represents different expression of yeast cell surface adhesion receptors or differential engagement of the endothelial endocytic machinery. Studies are ongoing to determine if differential uptake is matched by differential adhesiveness and if such differences are reflected in their pathogenicity. This result indicates that differences between isolates are a considerable source of variation in studies of host interaction with *C. parapsilosis*. The Als3p adhesin of *C. albicans* has been shown to
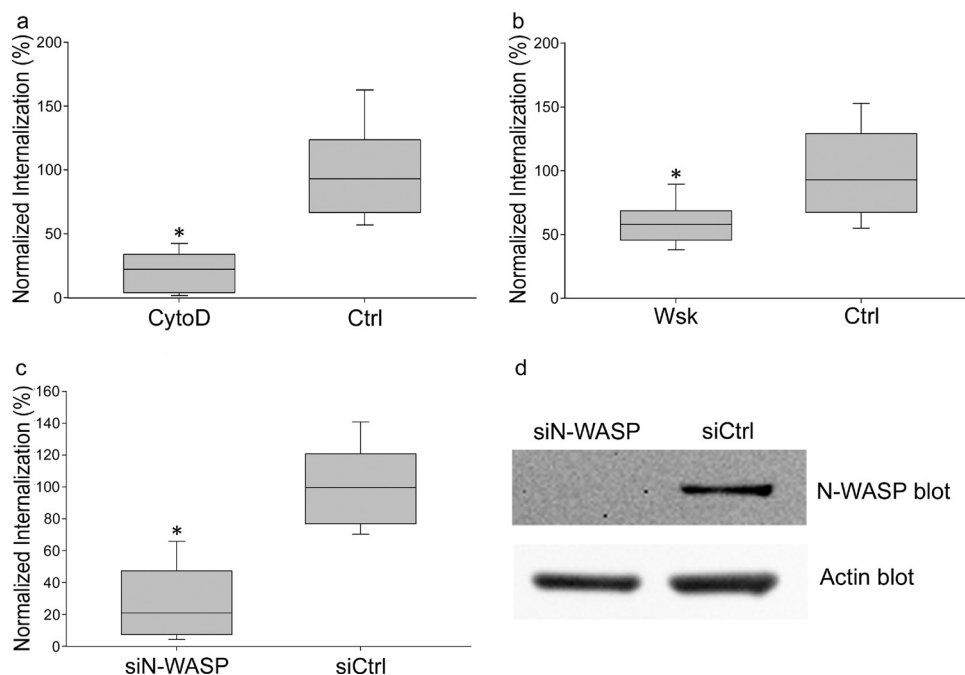
FIG 5 (a) Cytochalasin D (CytoD) blocked internalization of heat-killed, pHrodo-labeled *C. parapsilosis*. HUVEC were incubated overnight with pHrodo-labeled *C. parapsilosis* JMB81 in the presence of 0.5 μM cytochalasin D. The graph represents the medians, 25th and 75th percentiles (boxes), and 10th and 90th percentiles (whiskers) from 3 independent experiments. *, $P < 0.001$ versus the control (Ctrl). (b) Wiskostatin blocked internalization of *C. parapsilosis* JMB81. HUVEC were incubated overnight with heat-killed pHrodo yeast in the presence of 2.5 μM wiskostatin (Wsk). The graph represents the medians, 25th and 75th percentiles (boxes), and 10th and 90th percentiles (whiskers) from 3 independent experiments. *, $P < 0.001$ versus the Ctrl. (c) siRNA for N-WASP blocked internalization of *C. parapsilosis*. HUVEC were transiently transfected with siRNA as described in Materials and Methods. Forty-eight h later, heat-killed, pHrodo-labeled JMB81 cells were added and incubated overnight. Monolayers were imaged at 72 h after siRNA transfection, at a time of maximal knockdown of N-WASP protein. The graph represents the medians, 25th and 75th percentiles (boxes), and 10th and 90th percentiles (whiskers) from 3 independent experiments. *, $P < 0.001$. (d) Western blot showing that N-WASP was knocked down following transient transfection of HUVEC with siRNA to N-WASP (siN-WASP) but not by control siRNA (siCtrl). Densitometry of the Western blot showed 71% knockdown when normalized to actin expression.

bind endothelial proteins, including N-cadherin, and Als protein orthologs have been identified in *C. parapsilosis* (21). However, indirect immunofluorescence experiments did not show N-cadherin localizing to adhesion sites of *C. parapsilosis* (data not shown), suggesting the potential for alternative adhesion mechanisms. For *C. parapsilosis*, the process of heat killing and pHrodo labeling did not markedly alter their uptake (compare Fig. 1a and b); however, this was not true for *C. albicans* (compare Fig. 8a and b). This observation suggests that *C. albicans* adhesin(s) is more sensitive to the heat-killing/pHrodo-labeling process than that of *C. parapsilosis*. Indeed, Phan et al. reported that when *C. albicans* germ tubes were killed with methanol rather than heat, 70% of the cell-associated organisms were endocytosed by endothelial cells within 3 h (12). Comparison of live JMB81 to live SC5314 showed roughly similar efficiency of internalization, but accurate comparison is difficult because of their different morphologies. Nevertheless, it is reasonable to conclude that lack of hyphal formation does not prevent rapid and efficient internalization of *C. parapsilosis* by endothelial cells.

Heat-killed *C. parapsilosis* yeast were transported into an acidic subcompartment of the endolysosomal pathway. Live *C. parapsilosis* may be similarly trafficked, but in macrophages, endocytosed live *C. glabrata* has been shown to resist acidification and killing and instead proliferates intracellularly in the host (37). In experiments with both live and heat-killed *C. parapsilosis*, internalized yeast were usually observed as clusters of 25 to 50 cells within an endothelial cell. Although clusters of *C. parapsilosis* were engulfed, occasional single yeast were also endocytosed with similar time courses. In some instances, yeast were observed to be taken up at different locations of the endothelial cell but brought close together after uptake (not shown). In Movie S2 in the supplemental material, a cluster of yeast are observed to transition to pHrodo bright. The entire cluster does not change fluorescence in synchrony; instead, yeast become acidified a few at a time. This result suggests that there is a diffusion barrier between adjacent yeast in a cluster, and they may reside in separate compartments or vesicles.

In endothelial cells it is not clear if internalized *C. parapsilosis* cells remain alive and metabolically active. We did not observe active *C. parapsilosis* replication within HUVEC by live cell imaging (Fig. 4; also see Movie S1 in the supplemental material); however, this may be occurring outside our 4-h observation window. In contrast, *C. albicans* underwent hyphal germination before, and elongation after, internalization. Internalized *C. parapsilosis* may also secrete proteases or lipases, leading to damage of the endothelial monolayer. Production of hydrolytic enzymes has been demonstrated to have a role in virulence in both *C. parapsilosis* (38, 39) and *C. albicans* (15). Endothelial damage, retraction, and shedding might result in exposure of the vascular basement membrane to circulating yeast. Another possibility is that endocytosed yeast are transported across the endothelial monolayer to be released at the basolateral surface toward tissues. Endothelial
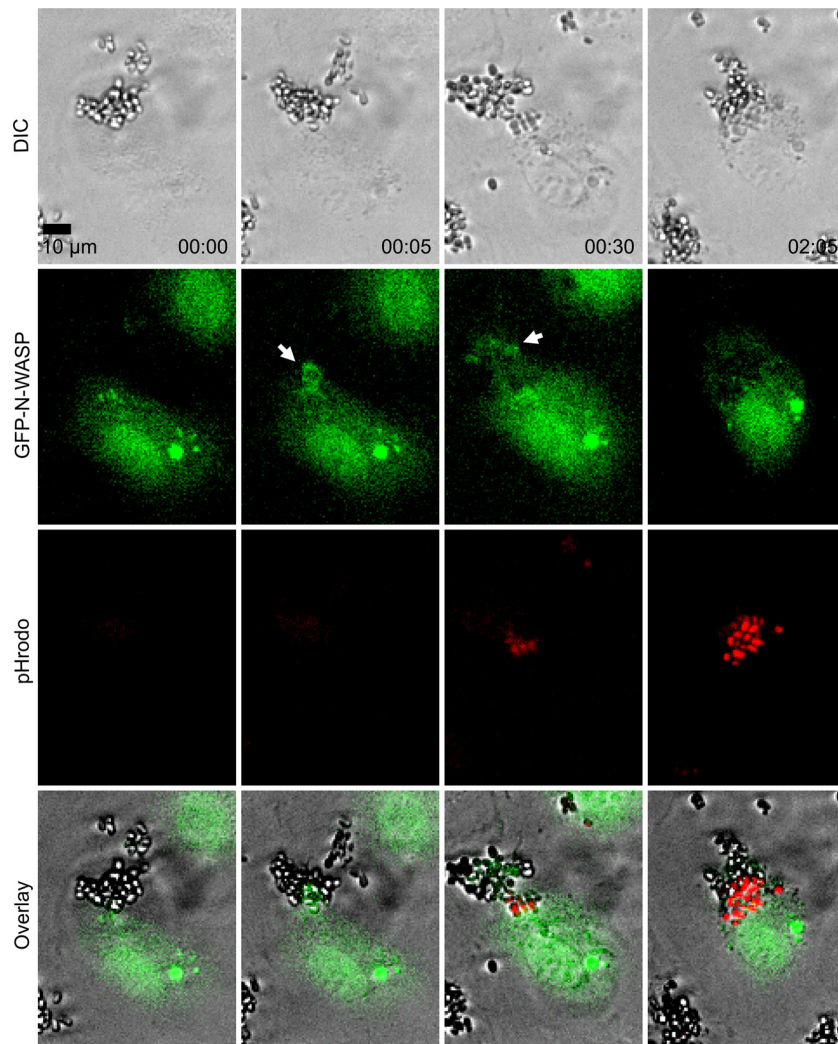
FIG 6 GFP-N-WASP localized to internalizing heat-killed, pHrodo-labeled *C. parapsilosis* (JMB81). The top row shows DIC images, the second row shows GFP-N-WASP, the third row shows pHrodo, and the fourth row shows overlays. Time is shown in hours and minutes. White arrows mark N-WASP clustering. Data are also shown in Movie S2 in the supplemental material, where localization of GFP-N-WASP may be more easily observed over time. Each image is representative of 2 independent experiments.

cells actively transport fluid and macromolecules across the monolayer by transcytosis, and this machinery may be hijacked by invading yeast.

Bovine serum increases uptake of yeast, but opsonization with serum factors was not sufficient to cause endocytosis. Thus, serum appears to directly stimulate endothelial endocytosis of *C. parapsilosis*, although the nature of the serum component responsible for this activity is not currently known. Serum and growth factors are well known to stimulate activity of cdc42 and Rac and may influence N-WASP activity and cytoskeletal rearrangement necessary for endocytosis. This result is in contrast to that for *C. albicans*, where endocytosis of hyphae was not altered by fetal bovine serum (FBS) (23). The actin cytoskeleton and N-WASP were involved in internalization of *C. parapsilosis*. Both components were recruited to sites of internalization, and internalization was blocked by pharmacological inhibition of actin nucleation or N-WASP. It was not possible to test siRNA or pharmacologic blockade of N-WASP with *C. albicans* because of the greatly re-

duced internalization of heat-killed, pHrodo-labeled SC5314. The role of N-WASP was instead confirmed by a FRET reporter of N-WASP activity, which showed active N-WASP throughout the internalization process, from early adhesion of yeast to the endothelial surface through vesicle formation and acidification. N-WASP activity was observed for endocytosis of both live and heat-killed yeast. Similar results were observed with *C. albicans* and *C. parapsilosis*. Thus, actin polymerization by N-WASP may represent a common mechanism for yeast internalization. N-WASP activity was observed around hyphae during adhesion of *C. albicans*, but at later points the activity encompassed the entire structure, including the parent yeast form. This observation suggests that in *C. albicans*, an adhesion molecule(s) that ultimately recruits N-WASP and results in actin polymerization is present on both hyphae and on the parent yeast. Although Als3 is present preferentially on hyphae, other adhesins are present on both yeast and hyphae (16) and may serve to trigger N-WASP activation.
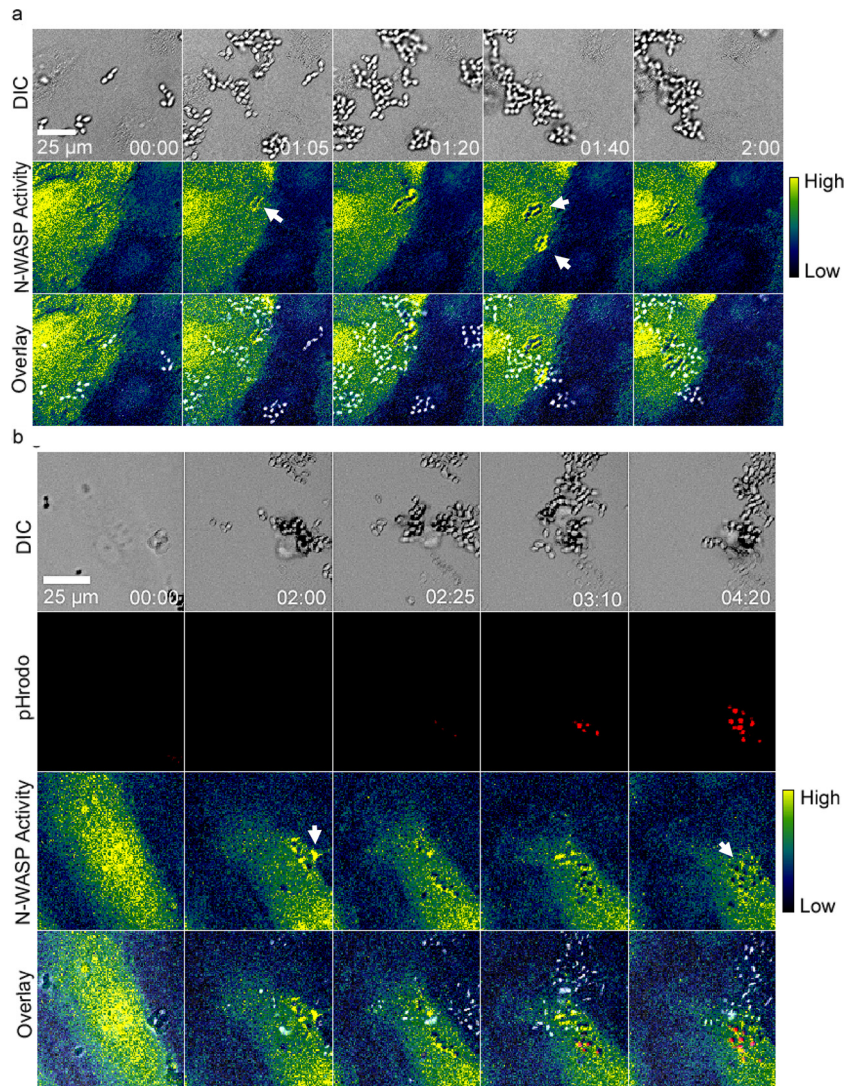
FIG 7 (a) N-WASP biosensor showed active N-WASP around internalizing live *C. parapsilosis* JMB81. The top row shows DIC, the middle row shows FRET (pseudocolor), and the bottom row shows overlays. White arrows show regions of N-WASP activity around internalizing yeast. A scale bar showing relative activity of N-WASP is shown on the right. Data are also shown in Movie S3 in the supplemental material. Image sequences are representative of 3 independent experiments. (b) pHrodo labeling showed that N-WASP activity occurred prior to internalization and persisted after transport to an acidic subcompartment for heat-killed *C. parapsilosis* JMB81. The top row shows DIC images, the second row shows pHrodo, the third row shows FRET (pseudocolor), and the fourth row shows overlays. White arrows show regions of N-WASP activity around internalizing yeast. Time is shown in hours and minutes. Movie S4 in supplementary data. Image sequences are representative of 5 independent experiments.

Other pathogens, such as *Shigella* (40) and enterohemorrhagic *Escherichia coli* (41), have been shown to require N-WASP-mediated actin polymerization, but the current study is the first report showing its role in internalization for *Candida*. These findings suggest that N-WASP plays a central role in internalization of pathogenic microorganisms. Other *Candida* species relevant to human disease, including *C. krusei* and *C. glabrata*, may also utilize similar pathways to gain access to host tissues beyond the bloodstream. For both *Shigella* and *E. coli*, bacterial proteins directly recruit host cytoskeletal elements, leading to nucleation of microfilaments. Cortactin is another nucleation promotion factor that has been shown to play a role in pathogenesis of many other organisms, including *Shigella*, *Neisseria*, *Listeria*, *Staphylococcus*, *E. coli*, and *Helicobacter pylori* (42). Cortactin is recruited to sites

of Als3p-mediated adhesion of *C. albicans* and is required for internalization of hyphae (28). Since cortactin is thought to cooperate with N-WASP in numerous models of actin nucleation (43, 44), we speculate that it also is necessary for *C. parapsilosis* internalization. Both N-WASP and the closely related WASP are required for macrophage phagocytosis via the Fcγ receptor (45), and WASP is localized to the phagocytic cup. N-WASP is activated by binding of cdc42 and PI(4,5)P2 (46). It is likely that small GTPases and acidic phospholipids are required for N-WASP activation during the endocytosis of *C. parapsilosis* described here. In the current study, scanning EM revealed sheet-like membrane extensions wrapping around adherent yeast. N-WASP is generally thought to be important for endocytosis of cell surface receptors (47) as well as for formation of leading edges of pseudopodia and
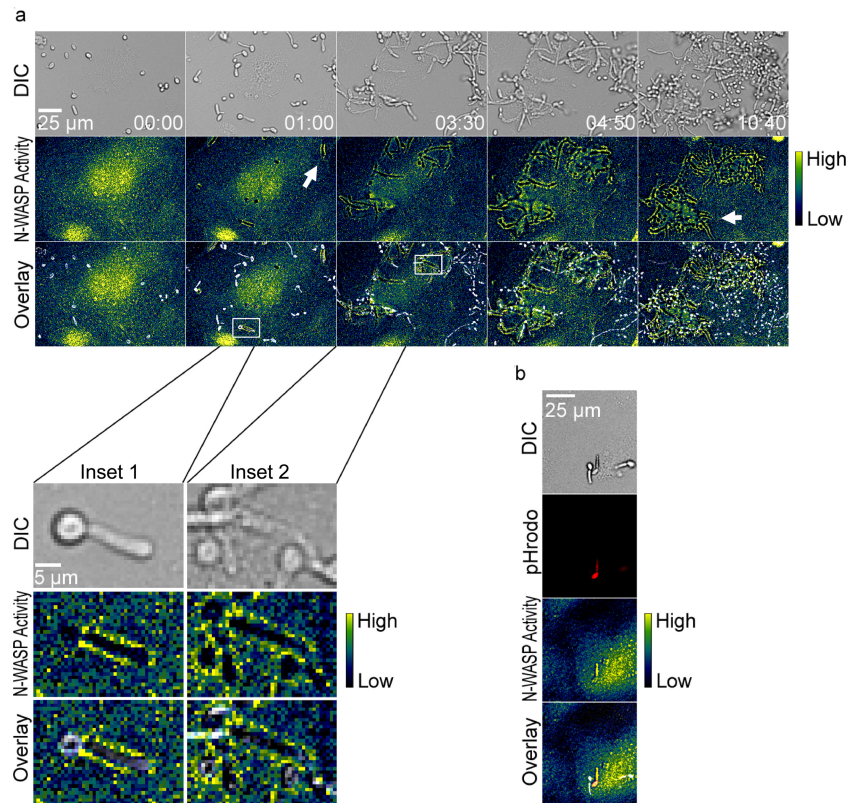
FIG 8 (a) N-WASP activity also occurred at sites of internalization of live *C. albicans* SC5314. The top row shows DIC images, the middle row shows FRET (pseudocolor), and the bottom row shows overlays. A scale bar showing relative activity of N-WASP is shown on the right. White arrows show regions of N-WASP activity around internalizing yeast. Data are also shown in Movie S5 in the supplemental material. Inset 1 shows an enlargement from the 1-h time point, where N-WASP activity is observed around the germ tube but not around the mother cell. Inset 2 shows a later time point, when N-WASP activity is observed around both the germ tube and mother cell. Image sequences are representative of 3 independent experiments. (b) N-WASP activity occurs for internalization of pHrodo-labeled, heat-killed *C. albicans* hyphae. Here, N-WASP activity is observed around the internalized pHrodo-bright yeast but not for the adjacent pHrodo-dim yeast. Images are representative of 5 independent experiments.

lamellipodia (31). Thus, the observed membrane extensions may be a direct result of N-WASP polymerizing activity.

In conclusion, our results indicate that adhesion of *C. parapsilosis* and *C. albicans* to endothelial cells leads to recruitment and activation of N-WASP. This results in nucleation of actin microfilaments and the envelopment of yeast by endothelial cell membranes. The process of internalization is rapid and efficient *in vitro* for both *C. albicans* and *C. parapsilosis* and may represent a mechanism of traversal of the blood vessel wall during candidiasis *in vivo*. Although the pathogenicity and prevalence of different *Candida* species is likely to be the result of multiple adaptations, N-WASP may play a common role in their internalization.

REFERENCES

1. **Stoll BJ, Hansen N, Fanaroff AA, Wright LL, Carlo WA, Ehrenkranz RA, Lemons JA, Donovan EF, Stark AR, Tyson JE, Oh W, Bauer CR, Korones SB, Shankaran S, Laptook AR, Stevenson DK, Papile LA, Poole WK.** 2002. Late-onset sepsis in very low birth weight neonates: the experience of the NICHD Neonatal Research Network. Pediatrics **110:**285–291.

2. **Wisplinghoff H, Bischoff T, Tallent SM, Seifert H, Wenzel RP, Edmond MB.** 2004. Nosocomial bloodstream infections in US hospitals: analysis of 24,179 cases from a prospective nationwide surveillance study. Clin. Infect. Dis. **39:**309–317.

3. **Benjamin DK, Jr, Stoll BJ, Fanaroff AA, McDonald SA, Oh W, Higgins RD, Duara S, Poole K, Laptook A, Goldberg R.** 2006. Neonatal candidiasis among extremely low birth weight infants: risk factors, mortality rates, and neurodevelopmental outcomes at 18 to 22 months. Pediatrics **117:**84–92.

4. **Pfaller MA, Diekema DJ.** 2007. Epidemiology of invasive candidiasis: a persistent public health problem. Clin. Microbiol. Rev. **20:**133–163.

5. **Beck-Sague C, Jarvis WR.** 1993. Secular trends in the epidemiology of nosocomial fungal infections in the United States, 1980–1990. National Nosocomial Infections Surveillance System. J. Infect. Dis. **167:**1247–1251.

6. **Chow BD, Linden JR, Bliss JM.** 2012. Candida parapsilosis and the neonate: epidemiology, virulence and host defense in a unique patient setting. Expert Rev. Anti Infect. Ther. **10:**935–946.

7. **Silva S, Negri M, Henriques M, Oliveira R, Williams DW, Azeredo J.** 2012. Candida glabrata, Candida parapsilosis and Candida tropicalis: biology, epidemiology, pathogenicity and antifungal resistance. FEMS Microbiol. Rev. **36:**288–305.

8. **Trofa D, Gacser A, Nosanchuk JD.** 2008. Candida parapsilosis, an emerging fungal pathogen. Clin. Microbiol. Rev. **21**:606–625.

9. **Neu N, Malik M, Lunding A, Whittier S, Alba L, Kubin C, Saiman L.** 2009. Epidemiology of candidemia at a children's hospital, 2002 to 2006. Pediatr. Infect. Dis. J. **28**:806–809.

10. **Pfaller MA, Diekema DJ, Jones RN, Sader HS, Fluit AC, Hollis RJ, Messer SA.** 2001. International surveillance of bloodstream infections due to Candida species: frequency of occurrence and in vitro susceptibilities to fluconazole, ravuconazole, and voriconazole of isolates collected from 1997 through 1999 in the SENTRY antimicrobial surveillance program. J. Clin. Microbiol. **39**:3254–3259.

11. **Saville SP, Lazzell AL, Monteagudo C, Lopez-Ribot JL.** 2003. Engineered control of cell morphology in vivo reveals distinct roles for yeast and filamentous forms of Candida albicans during infection. Eukaryot. Cell **2**:1053–1060.

12. **Phan QT, Belanger PH, Filler SG.** 2000. Role of hyphal formation in interactions of Candida albicans with endothelial cells. Infect. Immun. **68**:3485–3490.

13. **Grubb SE, Murdoch C, Sudbery PE, Saville SP, Lopez-Ribot JL, Thornhill MH.** 2009. Adhesion of Candida albicans to endothelial cells under physiological conditions of flow. Infect. Immun. **77**:3872–3878.

14. **Hoyer LL.** 2001. The ALS gene family of Candida albicans. Trends Microbiol. **9**:176–180.

15. **Zhu W, Filler SG.** 2010. Interactions of Candida albicans with epithelial cells. Cell Microbiol. **12**:273–282.

16. **Grubb SE, Murdoch C, Sudbery PE, Saville SP, Lopez-Ribot JL, Thornhill MH.** 2008. Candida albicans-endothelial cell interactions: a key step in the pathogenesis of systemic candidiasis. Infect. Immun. **76**:4370–4377.

17. **Liu Y, Filler SG.** 2011. Candida albicans Als3, a multifunctional adhesin and invasin. Eukaryot. Cell **10**:168–173.

18. **Phan QT, Fratti RA, Prasadarao NV, Edwards JE, Jr, Filler SG.** 2005. N-cadherin mediates endocytosis of Candida albicans by endothelial cells. J. Biol. Chem. **280**:10455–10461.

19. **Zhu W, Phan QT, Boontheung P, Solis NV, Loo JA, Filler SG.** 2012. EGFR and HER2 receptor kinase signaling mediate epithelial cell invasion by Candida albicans during oropharyngeal infection. Proc. Natl. Acad. Sci. U. S. A. **109**:14194–14199.

20. **Zupancic ML, Frieman M, Smith D, Alvarez RA, Cummings RD, Cormack BP.** 2008. Glycan microarray analysis of Candida glabrata adhesin ligand specificity. Mol. Microbiol. **68**:547–559.

21. **Butler G, Rasmussen MD, Lin MF, Santos MA, Sakthikumar S, Munro CA, Rheinbay E, Grabherr M, Forche A, Reedy JL, Agrafioti I, Arnaud MB, Bates S, Brown AJ, Brunke S, Costanzo MC, Fitzpatrick DA, de Groot PW, Harris D, Hoyer LL, Hube B, Klis FM, Kodira C, Lennard N, Logue ME, Martin R, Neiman AM, Nikolaou E, Quail MA, Quinn J, Santos MC, Schmitzberger FF, Sherlock G, Shah P, Silverstein KA, Skrzypek MS, Soll D, Staggs R, Stansfield I, Stumpf MP, Sudbery PE, Srikantha T, Zeng Q, Berman J, Berriman M, Heitman J, Gow NA, Lorenz MC, Birren BW, Kellis M, Cuomo CA.** 2009. Evolution of pathogenicity and sexual reproduction in eight Candida genomes. Nature **459**:657–662.

22. **Park H, Myers CL, Sheppard DC, Phan QT, Sanchez AA, Edwards JE, Filler SG.** 2005. Role of the fungal Ras-protein kinase A pathway in governing epithelial cell interactions during oropharyngeal candidiasis. Cell Microbiol. **7**:499–510.

23. **Wachtler B, Citiulo F, Jablonowski N, Forster S, Dalle F, Schaller M, Wilson D, Hube B.** 2012. Candida albicans-epithelial interactions: dissecting the roles of active penetration, induced endocytosis and host factors on the infection process. PLoS One **7**:e36952. doi:10.1371/journal.pone.0036952.

24. **Jong AY, Stins MF, Huang SH, Chen SH, Kim KS.** 2001. Traversal of Candida albicans across human blood-brain barrier in vitro. Infect. Immun. **69**:4536–4544.

25. **Klotz SA, Drutz DJ, Harrison JL, Huppert M.** 1983. Adherence and penetration of vascular endothelium by Candida yeasts. Infect. Immun. **42**:374–384.

26. **Lossinsky AS, Jong A, Fiala M, Mukhtar M, Buttle KF, Ingram M.** 2006. The histopathology of Candida albicans invasion in neonatal rat tissues and in the human blood-brain barrier in culture revealed by light, scanning, transmission and immunoelectron microscopy. Histol. Histopathol. **21**:1029–1041.

27. **Rotrosen D, Edwards JE, Jr, Gibson TR, Moore JC, Cohen AH, Green I.** 1985. Adherence of Candida to cultured vascular endothelial cells: mechanisms of attachment and endothelial cell penetration. J. Infect. Dis. **152**:1264–1274.

28. **Moreno-Ruiz E, Galan-Diez M, Zhu W, Fernandez-Ruiz E, d'Enfert C, Filler SG, Cossart P, Veiga E.** 2009. Candida albicans internalization by host cells is mediated by a clathrin-dependent mechanism. Cell Microbiol. **11**:1179–1189.

29. **Ballestrem C, Wehrle-Haller B, Imhof BA.** 1998. Actin dynamics in living mammalian cells. J. Cell Sci. **111**(Part 12):1649–1658.

30. **Parsons M, Monypenny J, Ameer-Beg SM, Millard TH, Machesky LM, Peter M, Keppler MD, Schiavo G, Watson R, Chernoff J, Zicha D, Vojnovic B, Ng T.** 2005. Spatially distinct binding of Cdc42 to PAK1 and N-WASP in breast carcinoma cells. Mol. Cell Biol. **25**:1680–1695.

31. **Lorenz M, Yamaguchi H, Wang Y, Singer RH, Condeelis J.** 2004. Imaging sites of N-wasp activity in lamellipodia and invadopodia of carcinoma cells. Curr. Biol. **14**:697–703.

32. **Wang X, Zeng W, Murakawa M, Freeman MW, Seed B.** 2000. Episomal segregation of the adenovirus enhancer sequence by conditional genome rearrangement abrogates late viral gene expression. J. Virol. **74**:11290–11303.

33. **Shaw SK, Bamba PS, Perkins BN, Luscinskas FW.** 2001. Real-time imaging of vascular endothelial-cadherin during leukocyte transmigration across endothelium. J. Immunol. **167**:2323–2330.

34. **Bliss JM, Basavegowda KP, Watson WJ, Sheikh AU, Ryan RM.** 2008. Vertical and horizontal transmission of Candida albicans in very low birth weight infants using DNA fingerprinting techniques. Pediatr. Infect. Dis. J. **27**:231–235.

35. **Benjamin DK, Jr, Stoll BJ, Gantz MG, Walsh MC, Sanchez PJ, Das A, Shankaran S, Higgins RD, Auten KJ, Miller NA, Walsh TJ, Laptook AR, Carlo WA, Kennedy KA, Finer NN, Duara S, Schibler K, Chapman RL, Van Meurs KP, IDFrantz, III, Phelps DL, Poindexter BB, Bell EF, O'Shea TM, Watterberg KL, Goldberg RN.** 2010. Neonatal candidiasis: epidemiology, risk factors, and clinical judgment. Pediatrics **126**:e865–873.

36. **Peterson JR, Bickford LC, Morgan D, Kim AS, Ouerfelli O, Kirschner MW, Rosen MK.** 2004. Chemical inhibition of N-WASP by stabilization of a native autoinhibited conformation. Nat. Struct. Mol. Biol. **11**:747–755.

37. **Seider K, Brunke S, Schild L, Jablonowski N, Wilson D, Majer O, Barz D, Haas A, Kuchler K, Schaller M, Hube B.** 2011. The facultative intracellular pathogen Candida glabrata subverts macrophage cytokine production and phagolysosome maturation. J. Immunol. **187**:3072–3086.

38. **Gacser A, Trofa D, Schafer W, Nosanchuk JD.** 2007. Targeted gene deletion in Candida parapsilosis demonstrates the role of secreted lipase in virulence. J. Clin. Investig. **117**:3049–3058.

39. **Trofa D, Soghier L, Long C, Nosanchuk JD, Gacser A, Goldman DL.** 2011. A rat model of neonatal candidiasis demonstrates the importance of lipases as virulence factors for Candida albicans and Candida parapsilosis. Mycopathologia **172**:169–178.

40. **Suzuki T, Miki H, Takenawa T, Sasakawa C.** 1998. Neural Wiskott-Aldrich syndrome protein is implicated in the actin-based motility of Shigella flexneri. EMBO J. **17**:2767–2776.

41. **Vingadassalom D, Campellone KG, Brady MJ, Skehan B, Battle SE, Robbins D, Kapoor A, Hecht G, Snapper SB, Leong JM.** 2010. Enterohemorrhagic E. coli requires N-WASP for efficient type III translocation but not for EspFU-mediated actin pedestal formation. PLoS Pathog. **6**:e1001056. doi:10.1371/journal.ppat.1001056.

42. **Selbach M, Backert S.** 2005. Cortactin: an Achilles' heel of the actin cytoskeleton targeted by pathogens. Trends Microbiol. **13**:181–189.

43. **Cosen-Binker LI, Kapus A.** 2006. Cortactin: the gray eminence of the cytoskeleton. Physiology (Bethesda) **21**:352–361.

44. **Ren G, Crampton MS, Yap AS.** 2009. Cortactin: coordinating adhesion and the actin cytoskeleton at cellular protrusions. Cell Motil. Cytoskeleton **66**:865–873.

45. **Park H, Cox D.** 2009. Cdc42 regulates Fc gamma receptor-mediated phagocytosis through the activation and phosphorylation of Wiskott-Aldrich syndrome protein (WASP) and neural-WASP. Mol. Biol. Cell **20**:4500–4508.

46. **Rohatgi R, Ho HY, Kirschner MW.** 2000. Mechanism of N-WASP activation by CDC42 and phosphatidylinositol 4, 5-bisphosphate. J. Cell Biol. **150**:1299–1310.

47. **Burianek LE, Soderling SH.** 2013. Under lock and key: spatiotemporal regulation of WASP family proteins coordinates separate dynamic cellular processes. Semin. Cell Dev. Biol. **24**:258–266.